Journal of Applied Mechanics Vol.8, pp.361-366 (August 2005) JSCE

Antisymmetric Bifurcation in Elastoplastic Cylinders under Uniaxial Compression

Mehdi KHOJASTEHPOUR*, Yukitaka MURAKAMI** and Koichi HASHIGUCHI***

* JSPS Postdoctoral Fellow, Dept. Mechanical Eng. Sci., Kyushu Univ. (Higashi-ku, Fukuoka 812-8581, Japan)
* Ph.D., Assistant Professor, Dept. Agricultural Eng., Ferdowsi Univ. of Mashhad, (Mashhad, Iran)
** Dr. Eng., Professor, Dept. Mechanical Eng. Sci, Kyushu Univ. (Higashi-ku, Fukuoka 812-8581, Japan)
*** Dr. Eng. and Dr. Agr., Professor, Dept. Bioproduction Environmental. Sci., Kyushu Univ. (Higashi-ku, Fukuoka 812-8581, Japan)

This article examines the localized and diffuse bifurcations of deformation in an incompressible circular cylinder subjected to axisymmetric loading consisting of the tangential-subloading surface model. The analysis considers the conditions for shear band formation, diffuse buckling formation, and the long and short wavelength limits of diffuse buckling modes in relation to material properties and stress. The effects of the normal-yield ratio describing the degree of approach to the normal-yield state and the tangential-plastic strain rate due to the tangential-stress rate effect on the diffuse bifurcations are discussed in details. It is revealed that the normal-yield ratio and the tangential strain rate influence the onset of diffuse bifurcation.

Keywords: *elastoplasticity, stability and bifurcation, subloading surface model*

1. Introduction

Various theoretical analyses for the material bifurcations and instabilities representing explanations for failure of materials have been presented in recent years, cf. e.g. Bardet[1], Chau[2, 3], Chau and Choi[4], Chau and Rudnicki[5], Cheng et al.[6], Durban and Papanastasiou[7], Hill and Hutchinson[12], Hutchinson and Miles[14], Miles[17], Miles and Nuwayhid[18], Needleman[19], Vardoulakis[24, 25], Yatomi and Shibi[26] and Young[27]. The deformation theory adopted by most of them is limited to the stress path near the proportional loading, violating the continuity condition for a stress path tangential to the yield surface since it encloses a purely elastic domain, exhibiting the abrupt transition from the elastic to the plastic state. Recently, Hashiguchi and Tsutsumi[8] have extended Rudnicki and Rice's constitutive model[20] so as to be applicable to the description of deformation behavior under arbitrary loading process for materials with arbitrary yield surface by introducing the tangential-strain rate. It was verified that the tangential-subloading surface model can predict appropriately the onset condition of bifurcations for soils[9, 15] and metals[10, 16].

This article extends and modifies the pervious antisymmetric bifurcation analyses of deformation in the cylindrical specimen[3, 26] to include tangential-subloading surface model[8]. The localized and diffuse bifurcation modes of a circular cylinder subjected to a compressive load are analyzed. The effects of the normal-yield ratio and the tangential-plastic strain rate on the formation of diffuse bifurcations are discussed in details.

2. Constitutive Relations

Consider a circular cylindrical specimen subjected to axial stress σ_{zz} at the frictionless ends, which yields the antisymmetric deformations (see Fig. 1). Deformation is postulated to be homogeneous up to the onset of bifurcation. Let the radius and the height be denoted by $\mathcal{R}$ and $\mathcal{H}$, respectively. The constitutive equation of the tangential-subloading surface model[8] for this case is expressed in the cylindrical coordinate system (r, θ, z) as follows:

$$\begin{aligned}
\overset{\circ}{\sigma}_{zz} &= 2\mu_n D_{zz},\\
\overset{\circ}{\sigma}_{rr} &= (\mu_n+\mu_t)D_{rr}+(\mu_n-\mu_t)D_{\theta\theta},\\
\overset{\circ}{\sigma}_{\theta\theta} &= (\mu_n-\mu_t)D_{rr}+(\mu_n+\mu_t)D_{\theta\theta},\\
\overset{\circ}{\sigma}_{r\theta} &= 2\mu_t D_{r\theta},\\
\overset{\circ}{\sigma}_{rz} &= 2\mu_t D_{rz},\\
\overset{\circ}{\sigma}_{\theta z} &= 2\mu_t D_{\theta z},
\end{aligned} \tag{1}$$

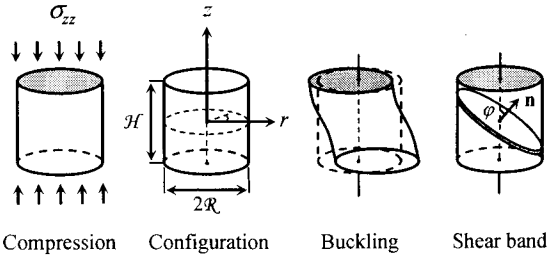

Fig. 1. The cylindrical specimen before and after deformation

where

$$D_{rr} + D_{\theta\theta} + D_{zz} = 0. \tag{2}$$

$\boldsymbol{\sigma}$ is the Cauchy stress tensor, $(\circ)$ denotes the Jaumann or co-rotational rate, and $\mathbf{D}$ is the rate of deformation tensor (the symmetric part of the velocity gradient). The instantaneous shear moduli μ_n and μ_t are given by

$$\mu_n = G\frac{M_p}{M_p + 2G} (\leq G), \tag{3}$$

$$\mu_t = G\frac{M_t}{M_t + 2G} (\leq G), \tag{4}$$

G is elastic shear modulus. The plastic modulus M_p and tangential modulus M_t according to tangential-subloading surface model for the simple elastoplastic material having von Mises yield condition with linear isotropic hardening[10] are defined as

$$M_p = (2/3)c_i R + \sqrt{2/3}UF, \quad U = -u_R \ln R, \tag{5}$$

$$F(H) = F_0(H) + c_i H, \tag{6}$$

$$M_t = TR^{-b}. \tag{7}$$

c_i, u_R, T and b are material constants, and F_0 is the initial value of the isotropic hardening function F with the argument of the isotropic hardening variable H. The degree of approach to the normal-yield state can be described by the normal-yield ratio $R\,(0 \leq R \leq 1)$ which is the size of the subloading surface to that of the normal-yield surface. For detailed discussion of tangential-subloading surface model, we refer to references 8-10.

3. Governing Equations

The continuing equilibrium equation in the absence of body forces is

$$\mathrm{div}\dot{\boldsymbol{\Pi}} = \mathbf{0}, \tag{8}$$

$(\bullet)$ stands for the material-time derivative. $\dot{\boldsymbol{\Pi}}$ is the nominal (first Piola-Kirchhoff) stress rate, it can be expressed in term of the Cauchy stress rate as follows:

$$\dot{\boldsymbol{\Pi}} = \overset{\circ}{\boldsymbol{\sigma}} + (\mathrm{tr}\mathbf{D})\boldsymbol{\sigma} - \boldsymbol{\sigma}\mathbf{D} + \mathbf{W}\boldsymbol{\sigma}, \tag{9}$$

Hereinafter, the Zaremba-Jaumann rate is used for the corotational rate of the stress $\boldsymbol{\sigma}$, i.e.

$$\overset{\circ}{\boldsymbol{\sigma}} = \dot{\boldsymbol{\sigma}} + \boldsymbol{\sigma}\mathbf{W} - \mathbf{W}\boldsymbol{\sigma}. \tag{10}$$

$\mathbf{W}$ is the spin tensor (the skew-symmetric part of the velocity gradient). For antisymmetric deformation, the nominal stress rate $\dot{\boldsymbol{\Pi}}$ in Eq. (9) can be expressed as

$$\dot{\Pi}_{rr} = \overset{\circ}{\sigma}_{rr}, \quad \dot{\Pi}_{rz} = \overset{\circ}{\sigma}_{rz} + \sigma(v_{r,z} - v_{z,r}),$$
$$\dot{\Pi}_{\theta r} = \overset{\circ}{\sigma}_{\theta r}, \quad \dot{\Pi}_{\theta z} = \overset{\circ}{\sigma}_{\theta z} + \sigma(v_{\theta,z} - r^{-1}v_{z,\theta}),$$
$$\dot{\Pi}_{r\theta} = \overset{\circ}{\sigma}_{r\theta}, \quad \dot{\Pi}_{z\theta} = \overset{\circ}{\sigma}_{z\theta} - \sigma(v_{\theta,z} + r^{-1}v_{z,\theta}),$$
$$\dot{\Pi}_{\theta\theta} = \overset{\circ}{\sigma}_{\theta\theta}, \quad \dot{\Pi}_{zr} = \overset{\circ}{\sigma}_{zr} - \sigma(v_{r,z} + v_{z,r}),$$
$$\dot{\Pi}_{zz} = \overset{\circ}{\sigma}_{rr} - 2\sigma v_{z,z}, \tag{11}$$

where

$$\sigma = \frac{1}{2}\sigma_{zz}. \tag{12}$$

$\mathbf{v}$ is the velocity, and the partial differentiation with respect to r, θ and z are denoted with $(\,)_{,r}$, $(\,)_{,\theta}$ and $(\,)_{,z}$, respectively.

In our research, we consider a purely homogeneous deformation process which proceeds up to the inception of bifurcation. We choose the cylindrical polar coordinate system (r, θ, z) such that the origin is located in the center of the cylinder and the z-axis coincides with the axis of symmetry (Fig. 1). On the ends, the specimen experiences compressive loading without shear traction. Eq. (8) in the cylindrical polar coordinates for our case reduces to

$$\dot{\Pi}_{rr,r} + r^{-1}\dot{\Pi}_{r\theta,\theta} + \dot{\Pi}_{rz,z} + r^{-1}(\dot{\Pi}_{rr} - \dot{\Pi}_{\theta\theta}) = 0,$$
$$r^{-1}\dot{\Pi}_{\theta\theta,\theta} + \dot{\Pi}_{\theta r,r} + \dot{\Pi}_{\theta z,z} + r^{-1}(\dot{\Pi}_{r\theta} + \dot{\Pi}_{\theta r}) = 0,$$
$$\dot{\Pi}_{zz,z} + \dot{\Pi}_{zr,r} + r^{-1}\dot{\Pi}_{z\theta,\theta} + r^{-1}\dot{\Pi}_{zr} = 0. \tag{13}$$

To solve the equilibrium equation (13), we employ the method of the velocity potentials proposed by Chau[3] that has been extended from the displacement potentials method[13, 21] for elastic problems. By modifying Chau's method, the modified velocity potentials $\Phi(r, \theta, z)$ and $\Psi(r, \theta, z)$ are proposed as follows:

$$v_r = \Phi_{,rz} + r^{-1}\Psi_{,\theta},$$
$$v_\theta = r^{-1}\Phi_{,\theta z} - \Psi_{,r},$$
$$v_z = -O_{r\theta}(\Phi), \tag{14}$$

where the operator $O_{r\theta}(\ )$ is defined as

$$O_{r\theta}(\ ) = (\ )_{,rr} + r^{-1}(\ )_{,r} + r^{-2}(\ )_{,\theta\theta}. \tag{15}$$

By substituting Eqs. (11) and (14) into Eq. (13), along with constitutive relations in Eq. (1), we obtain

$$(\mu_t - \sigma)O_{r\theta}^2(\Phi) + (3\mu_n - \mu_t)(O_{r\theta}(\Phi))_{,zz} + (\mu_t + \sigma)\Phi_{,zzzz} = 0,$$
$$\mu_t O_{r\theta}(\Psi) + (\mu_t + \sigma)\Psi_{,zz} = 0. \tag{16}$$

The relationships in Eq. (16) are the fourth and second order partial differential equations of the mixed type that can be elliptic, hyperbolic or parabolic depending on the state of stress and values of internal variables. The particular linearization described here yields a governing equation applicable to the tangential-subloading surface model.

4. Localized Bifurcation

Consider a purely homogeneous deformation process with progressing to the onset of shear band formation. The unit vector normal to the shear band is denoted by $\mathbf{n}\,(n_r, n_\theta, n_z)$ (Fig. 1). Two conditions, the geometrical compatibility and the incremental equilibrium across the

shear band, must be satisfied for the shear band formation. These conditions can be expressed as follows[11]:

$$\nabla \mathbf{v} = \mathbf{g} \otimes \mathbf{n}, \quad \overset{\bullet}{\mathbf{\Pi}} \mathbf{n} = 0. \tag{17}$$

where $\mathbf{g}$ is the jump vector of the velocity gradient. Substituting Eq. (11) into (17) with constitutive relations in Eq. (1) yields the following algebraic equation:

$$(\mu_t(n_r^2+n_\theta^2)+(\mu_t+\sigma)n_z^2)((\mu_t-\sigma)(n_r^2+n_\theta^2)^2 + (3\mu_n-\mu_t)(n_r^2+n_\theta^2)n_z^2+(\mu_t+\sigma)n_z^4)=0. \tag{18}$$

The condition for the formation of shear band is given as a loss of ellipticity of Eq. (18). The solutions of Eq. (18) are classified as the elliptic complex (EC), elliptic imaginary (EI), parabolic (P) and hyperbolic (H) regimes, according to the existence of zero, two, and four real roots, respectively. Assume the shear band be formed at EC-H boundary. Therefore, the inclination angle φ of the shear band may be obtained as

$$\varphi = \tan^{-1}\left(\frac{\mu_t+\sigma}{\mu_t-\sigma}\right)^{1/4}. \tag{19}$$

5. Diffuse Bifurcation

We investigate the possibility of diffuse bifurcations that precede localization for a cylindrical specimen with radius $\mathcal{R}$ and height $\mathcal{H}$ at the onset of bifurcation (Fig. 1). The specimen is subjected to current axial compressive stress σ_{zz} on the ends without friction. The velocity potentials $\Phi(r,\theta,z)$ and $\Psi(r,\theta,z)$, which give rise to the diffuse bifurcation modes are given by

$$\Phi(r,\theta,z)=\phi(r)\cos(\zeta z)\sin(n\theta),$$
$$\Psi(r,\theta,z)=\psi(r)\sin(\zeta z)\cos(n\theta), \tag{20}$$

where $\zeta = k\pi/\mathcal{H}$, with $k=1,2,3,\ldots$.

The boundary conditions on the sides can be written as

$$\overset{\bullet}{\Pi}_{rr}=0, \quad \overset{\bullet}{\Pi}_{zr}=0, \quad \overset{\bullet}{\Pi}_{\theta r}=0, \quad \text{on } r=\mathcal{R}. \tag{21}$$

The substitution of Eqs. (1), (11) and (20) into Eq. (13) allows the boundary conditions on the sides to be expressed as

$$\frac{d}{dr}O_r(\phi)+\zeta^2\frac{d\phi}{dr}+\frac{n}{r}\zeta\psi=0,$$
$$O_r(\psi)-2\left(\frac{1}{r}\frac{d}{dr}-\left(\frac{n}{r}\right)^2\right)\psi + 2n\zeta\left(\frac{1}{r}\frac{d}{dr}-\frac{1}{r^2}\right)\phi=0,$$
$$(\mu_t-\sigma)O_r^2(\phi)-\zeta^2(3\mu_n-\sigma)O_r(\phi) + 2\zeta^2\mu_t\left(\frac{1}{r}\frac{d}{dr}-\left(\frac{n}{r}\right)^2\right)\phi - 2n\zeta\mu_t\left(\frac{1}{r}\frac{d}{dr}-\frac{1}{r^2}\right)\psi=0, \tag{22}$$

where

$$O_r(\ )=\frac{d^2(\ )}{dr^2}+\frac{1}{r}\frac{d(\ )}{dr}-\left(\frac{n}{r}\right)^2(\ ). \tag{23}$$

If one substitutes the eigenmode of Eq. (20) into Eq. (16), the following governing differential equation for $\phi(r)$ and $\psi(r)$ can be obtained:

$$(\mu_t-\sigma)O_r^2(\phi)-\zeta^2(3\mu_n-\mu_t)O_r(\phi) + \zeta^4(\mu_t+\sigma)\phi=0,$$
$$\mu_t O_r(\psi)-\zeta^2(\mu_t+\sigma)\psi=0, \tag{24}$$

Alternatively, Eq. (24) can be written as:

$$(O_r+\zeta^2\xi_1^2)(O_r+\zeta^2\xi_2^2)\phi(r)=0,$$
$$(O_r-\zeta^2\xi_3^2)\psi(r)=0. \tag{25}$$

Eq. (25) can be rewritten as two Bessel's differential equations with respect to ξ_1 and ξ_2, and one modified Bessel's differential equation with respect to ξ_3. Since $\phi(r)$ and $\psi(r)$ should be finite at $r=0$, the general solutions of Eq. (24) or Eq. (25) have the form

$$\phi(r)=C_1J_1(\zeta\xi_1 r)+C_2J_1(\zeta\xi_2 r),$$
$$\psi(r)=C_3I_n(\zeta\xi_3 r), \tag{26}$$

where

$$\xi_3=\left(\frac{\mu_t+\sigma}{\mu_t}\right)^{1/2}, \tag{27}$$

C_1, C_2 and C_3 are constants. $J_1(\ )$ and $I_n(\ )$ are the Bessel function of the first kind and the first order, and the modified Bessel function of the first kind of order n, respectively. Further, ξ_1 and ξ_2 are the roots of the following characteristic equation:

$$(\mu_t-\sigma)\xi^4+(3\mu_n-\mu_t)\xi^2+(\mu_t+\sigma)=0. \tag{28}$$

The roots of Eq. (28) are classified as the elliptic complex (EC), the elliptic imaginary (EI), the hyperbolic (H) and the parabolic (P) regimes, dependent on the state of stress and values of internal variables. In each of these regimes, diffuse bifurcations are possible, and in each regime analysis leads to the appropriate eigenvalue equation. The solution of the eigenvalue equations is similar to that of equations for plane strain conditions[5,12], for axisymmrtric deformations[2,25] and for antisymmetric deformation[3], which the results with tangential-subloading surface model are summarized below.

5.1 Elliptic complex regime

The solutions (26) in the elliptic complex regime have the form (for $n=1$)

$$\phi(r)=\mathrm{Re}[C_1J_1(\zeta\xi r)],$$
$$\psi(r)=C_3I_1(\zeta\xi_3 r), \tag{29}$$

where Re[ ] denotes the real part of [ ]. $\xi=\alpha+i\beta$ and its conjugate $\bar{\xi}=\alpha-i\beta$, $(i=\sqrt{-1})$, are the roots of Eq. (28), and the quantities α and β satisfy the following equations:

$$\alpha^2+\beta^2=\left(\frac{\mu_t+\sigma}{\mu_t-\sigma}\right)^{1/2},$$

$$\alpha^2-\beta^2=-\frac{1}{2}\frac{3\mu_n-\mu_t}{\mu_t-\sigma}. \tag{30}$$

Substituting Eq. (29) into boundary conditions (22) leads to the following eigenvalue equation:

$$M_1\mathrm{Im}[f_1(\xi)f_3(\bar{\xi})]+M_2\mathrm{Im}[f_2(\bar{\xi})f_3(\xi)] +M_3\mathrm{Im}[f_1(\bar{\xi})f_2(\xi)]=0, \tag{31}$$

where Im[ ] denotes the imaginary part of [ ]. M_1, M_2 and M_3 are defined as:

$$\begin{aligned}M_1&=2I_1(\omega\xi_3),\\ M_2&=(\omega^2\xi_3^2+4)I_1(\omega\xi_3)-2\omega\xi_3 I_0(\omega\xi_3),\\ M_3&=4\mu_t(2I_1(\omega\xi_3)-\omega\xi_3 I_0(\omega\xi_3)),\end{aligned} \tag{32}$$

$\omega=\zeta\mathcal{R}=k\pi\mathcal{R}/\mathcal{H}$ is the wavelength, and the complex functions $f_1(\chi)$, $f_2(\chi)$ and $f_3(\chi)$ are given by:

$$\begin{aligned}f_1(\chi)&=\omega\chi J_0(\omega\chi)-2J_1(\omega\chi),\\ f_2(\chi)&=(1-\chi^2)(\omega\chi J_0(\omega\chi)-J_1(\omega\chi)),\\ f_3(\chi)&=((\mu_t-\sigma)\chi^2(\omega^2\chi^2+1)+(3\mu_n-\sigma)\omega^2\chi^2 -4\mu_t)J_1(\omega\chi)+2\mu_t\omega\chi J_0(\omega\chi).\end{aligned} \tag{33}$$

5.2 Elliptic imaginary regime

In the elliptic imaginary regime, the roots of Eq. (28) are $\xi_1=\pm i\alpha$ and $\xi_2=\pm i\beta$, and the general solutions (26) have the form (for $n=1$)

$$\begin{aligned}\phi(r)&=C_1I_1(\zeta\alpha r)+C_2I_1(\zeta\beta r),\\ \psi(r)&=C_3I_1(\zeta\xi_3 r),\end{aligned} \tag{34}$$

where α and β satisfy the following equations:

$$\begin{aligned}\alpha^2+\beta^2&=\frac{3\mu_n-\mu_t}{\mu_t-\sigma},\\ \alpha^2-\beta^2&=\frac{((3\mu_n-\mu_t)^2-4(\mu_t^2-\sigma^2))^{1/2}}{\mu_t-\sigma}.\end{aligned} \tag{35}$$

The substitution of Eq. (34) into the boundary conditions (22) yields the eigenvalue equation:

$$M_1[g_1(\alpha)g_3(\beta)-g_1(\beta)g_3(\alpha)] +M_2[g_2(\beta)g_3(\alpha)-g_2(\alpha)g_3(\beta)] +M_3[g_1(\beta)g_2(\alpha)-g_1(\alpha)g_2(\beta)]=0, \tag{36}$$

where M_1, M_2 and M_3 are the same as in Eq. (32), and the functions $g_1(\chi)$, $g_2(\chi)$ and $g_3(\chi)$ are defined as:

$$\begin{aligned}g_1(\chi)&=\omega\chi I_0(\omega\chi)-2I_1(\omega\chi),\\ g_2(\chi)&=(\chi^2+1)(\omega\chi I_0(\omega\chi)-I_1(\omega\chi)),\\ g_3(\chi)&=((\mu_t-\sigma)\chi^2(\omega^2\chi^2-1)-(3\mu_n-\sigma)\omega^2\chi^2 -4\mu_t)I_1(\omega\chi)+2\mu_t\omega\chi I_0(\omega\chi).\end{aligned} \tag{37}$$

5.3 Parabolic regime

The general solutions, Eq. (26), in the parabolic regime have the form (for $n=1$)

$$\begin{aligned}\phi(r)&=C_1J_1(\zeta\alpha r)+C_2I_1(\zeta\beta r),\\ \psi(r)&=C_3J_1(\zeta\xi_3 r),\end{aligned} \tag{38}$$

where $\xi_1=\pm\alpha$ and $\xi_2=\pm i\beta$ are the roots of Eq. (28) for the parabolic regime. α and β are defined as

$$\begin{aligned}\alpha^2+\beta^2&=\frac{((3\mu_n-\mu_t)^2-4(\mu_t^2-\sigma^2))^{1/2}}{|\mu_t-\sigma|},\\ \alpha^2-\beta^2&=-\frac{3\mu_n-\mu_t}{\mu_t-\sigma}.\end{aligned} \tag{39}$$

Substituting Eq. (38) into the boundary conditions (22) yields the following eigenvalue equation:

$$N_1[f_1(\alpha)g_3(\beta)-g_1(\beta)f_3(\alpha)] +N_2[g_2(\beta)f_3(\alpha)-f_2(\alpha)g_3(\beta)] +N_3[g_1(\beta)f_2(\alpha)-f_1(\alpha)g_2(\beta)]=0, \tag{40}$$

where N_1, N_2 and N_3 are defined as:

$$\begin{aligned}N_1&=2J_1(\omega\xi_3),\\ N_2&=(4-\omega^2\xi_3^2)J_1(\omega\xi_3)-2\omega\xi_3 J_0(\omega\xi_3),\\ N_3&=4\mu_t(2J_1(\omega\xi_3)-\omega\xi_3 J_0(\omega\xi_3)).\end{aligned} \tag{41}$$

5.4 Hyperbolic regime

Solutions of Eq. (26) in the hyperbolic have the form (for $n=1$)

$$\begin{aligned}\phi(r)&=C_1J_1(\zeta\alpha r)+C_2J_1(\zeta\beta r),\\ \psi(r)&=C_3I_1(\zeta\xi_3 r),\end{aligned} \tag{42}$$

In the hyperbolic regime, the roots of Eq. (28) are $\xi_1=\pm\alpha$ and $\xi_2=\pm\beta$, which α and β are defined as:

$$\begin{aligned}\alpha^2+\beta^2&=-\frac{3\mu_n-\mu_t}{\mu_t-\sigma},\\ \alpha^2-\beta^2&=\frac{((3\mu_n-\mu_t)^2-4(\mu_t^2-\sigma^2))^{1/2}}{\mu_t-\sigma}.\end{aligned} \tag{43}$$

The substitution of Eq. (42) into the boundary conditions (22) yields the eigenvalue equation:

$$M_1[f_1(\alpha)f_3(\beta)-f_1(\beta)f_3(\alpha)] +M_2[f_2(\beta)f_3(\alpha)-f_2(\alpha)f_3(\beta)] +M_3[f_1(\beta)f_2(\alpha)-f_1(\alpha)f_2(\beta)]=0. \tag{44}$$

6. Results and Discussions

The instantaneous shear modulus μ_n in Eq. (3) is independent of the tangential strain rate and gradually decreases from the elastic shear modulus G as the normal-yield ratio R increases, as shown in Fig. 2. The instantaneous shear modulus μ_t, in Eq. (4) is independent of the plastic strain rate and decreases monotonically with the increase of R, as shown in Fig. 2. A salient feature of the present formulation is that both plastic and tangential strain rate are induced gradually as the stress approaches the normal-yield surface, i.e. as $R\to 1$, fulfilling both the

continuity and smoothness conditions (Fig. 2). On the other hand, in conventional plasticity models with $u_R \to \infty$ and $T \to \infty$, μ_n and μ_t suddenly jump from the purely elastic response to the normal-yield response at the moment when the stress reaches the normal-yield surface.

Figure 3 represents the bifurcation regimes as a function of the dimensionless variables σ/μ_t and $3\mu_n/\mu_t$ by the specified regions; elliptic complex (EI), elliptic imaginary (EI), hyperbolic (H) and parabolic (P) regimes. Figures 4 and 5 represent the lowest bifurcation stress as a function of the wavelength of diffuse modes ω obtained for antisymmetric elliptic modes of bifurcation in several values of R and T, which the long wavelength limit ($\omega \to 0$) coincides with the σ/μ_t-axis. The lowest possible bifurcation stress is at $\omega = 0$; it rises more rapidly when ω is between one and two, then slowly increases as values of ω increase. The normal-yield ratio R influences the bifurcation stress, as the bifurcation is highly induced at $R > 0.95$, i.e. near the normal-yield state as shown in Fig. 4. The influence of the material constant T prescribing the intensity of the tangential-stress rate effect on the bifurcation stress is quite intense as shown in Fig. 5, which the normal-yield ratio at the onset of antisymmetric deformation is very close to unity.

Here, we consider only the long wavelength limit ($\omega \to 0$) and the short wavelength limit ($\omega \to \infty$) of the eigenvalue equation in EC and EI regimes. In the elliptic complex regime for the long wavelength limit ($\omega \to 0$), Eq. (31) leads to $\sigma \to 0$, and for small ω yields

$$\frac{\sigma}{3\mu_n} = \frac{1}{2^3}\omega^2 + \mathrm{O}(\omega^4). \tag{45}$$

Here, it should be noted that the first term on right-hand side of Eq. (45) corresponds to the Euler's buckling formula[23], if $k = 1$. The substitution of the asymptotic expansions of $J_0(\ )$, $J_1(\ )$, $I_0(\ )$ and $I_1(\ )$ with large arguments[22] into Eq. (31), for the short wavelength limit ($\omega \to \infty$) in the elliptic complex regime, yields

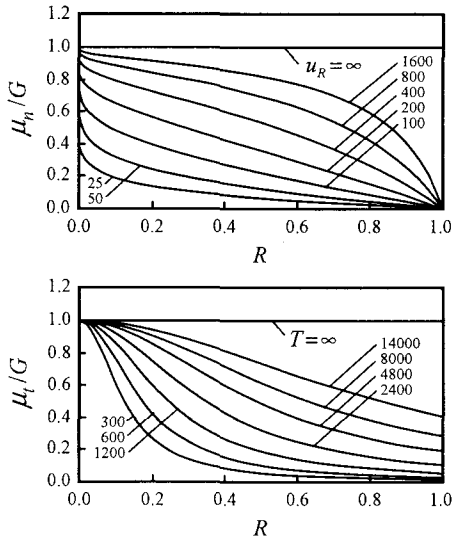

Fig. 2. Instantaneous shear moduli μ_n and μ_t vs. the normal-yield ratio R (c_i=75, b=2)

$$\frac{\sigma}{\mu_t} = \frac{1}{2} + \frac{1}{2}\frac{3\mu_n}{\mu_t} + \frac{\sigma}{\mu_t}\left(\frac{\mu_t - \sigma}{\mu_t + \sigma}\right)^{1/2}. \tag{46}$$

The $(\sigma/\mu_t, 3\mu_n/\mu_t)$ trajectories for the short wavelength limit ($\omega \to \infty$) (Eq. (46)) are shown in Fig. 3 by the dashed curve.

Considering the elliptic imaginary regime in the long wavelength limit ($\omega \to 0$), leads to $\sigma \to 0$ and for small ω produces Eq. (45) again. In the short wavelength limit ($\omega \to \infty$), the substitution of the asymptotic expansions of $I_0(\ )$ and $I_1(\ )$ for large arguments[22] into Eq. (36), again produces Eq. (46).

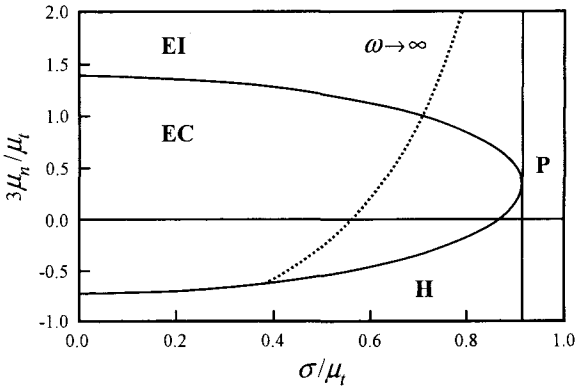

Fig. 3. Characteristic regimes of the diffuse bifurcation

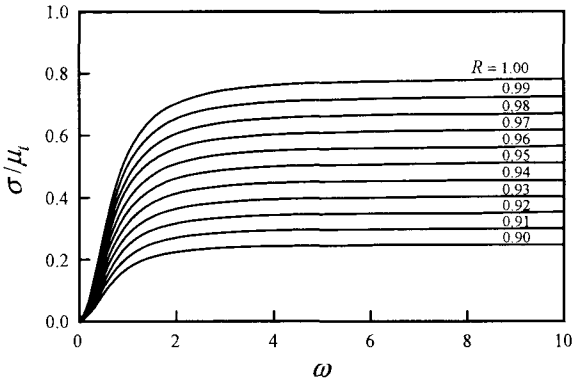

Fig. 4. Lowest bifurcation stress with the variation of normal-yield ratio R (u_R=100, c_i=50, T=500, b=2)

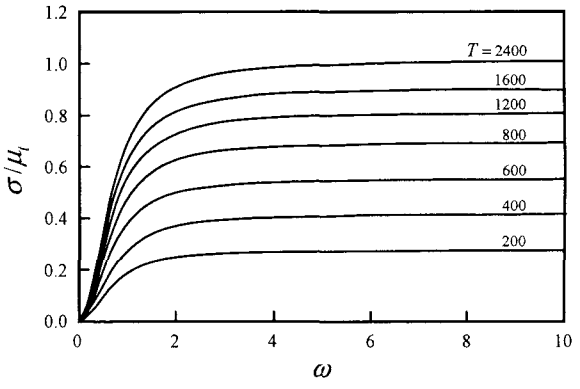

Fig. 5. Lowest bifurcation stress with the variation of material parameter T (R=1, u_R=200, c_i=75, b=2)

7. Concluding Remarks

Antisymmetric bifurcations of a cylindrical specimen subjected to the compressive load were analyzed by adopting the tangential-subloading surface model. Analytical solutions for the inception of localized bifurcation and antisymmetic diffuse modes were derived and classified into the elliptic complex, elliptic imaginary, hyperbolic and parabolic regimes. It was indicated that the normal-yield and the tangential strain rate term influence the formation of shear band and diffuse buckling modes.

Acknowledgment

The research in this paper was carried out while the first author was JSPS postdoctoral researcher at Kyushu University. This work was supported by Japan Society for the Promotion of Science (JSPS).

References

1) Bardet, J.P., Analytical solutions for the plane-strain bifurcation of compressible solids, *J. Appl. Mech. (ASME)* Vol. 58, pp. 651-657, 1991.
2) Chau, K.T., Non-normality and bifurcation in a compressible pressure-sensitive circular cylinder under axisymmetric tension and compression, *Int. J. of Solids Struct.*, Vol. 29, pp. 801-824, 1992.
3) Chau, K.T., Antisymmetric bifurcations in a compressible pressure-sensitive circular axisymmetric tension and compression, *J. Appl. Mech. (ASME)* Vol. 60, pp 282-289. 1993.
4) Chau K.T., Choi S.K., Bifurcations of thick-walled hollow cylinders of geomaterials under axisymmetric compression, *Int. J. Numer. Anal. Meth. Geomech.* Vol. 22, pp. 903-919, 1998.
5) Chau, K.T, and Rudnicki, J.W., Bifurcation of compressible pressure-sensitive materials in plane strain tension and compression, *J. Mech. Phys. Solids*, Vol. 38, pp. 875-898, 1990.
6) Cheng, S.Y., Ariaratnam, S.T. and Dubey, R.N., Axisymmetric bifurcation in an elastic-plastic cylinder under axial load and lateral hydrostatic pressure, *Quart. Appl. Math.*, Vol. 29, pp. 41-51, 1971.
7) Durban, D., Papanastasiou, P., Plastic bifurcation in the triaxial confining pressure test, *J. Appl. Mech. (ASME)*, Vol. 67, pp. 552-557, 2000.
8) Hashiguchi, K. and Tsutsumi, S., Elastoplastic constitutive equation with tangential stress rate effect, *Int. J. Plasticity*, Vol. 17, pp. 117-145, 2001.
9) Hashiguchi, K. and Tsutsumi, S., Shear band formation analysis in soils by the subloading surface model with tangential stress rate effect, *Int. J. Plasticity*, Vol. 19, pp. 1651-1677, 2003.
10) Hashiguchi, K. and Protasov, A., Localized necking analysis by the subloading surface model with tangential-strain rate and anisotropy, *Int. J. Plasticity*, Vol.20, pp. 1909-1930, 2004.
11) Hill, R., Discontinuity relations in mechanics of solids, *Progress in Solid Mechanics,* Vol. 2, pp. 246-276, 1961.
12) Hill, R. and Hutchinson, J.W., Bifurcation phenomena in the plane tension test, *J. Mech. Phys. Solids*, Vol. 23, pp. 239-264, 1975.
13) Hu, H.-C, On the three-dimensional problems of the theory of elasticity of a transversely isotropic body. *Acta Scientia Sincia*, Vol. 2, pp. 145-151, 1954.
14) Hutchinson, J.W. and Miles, J.P., Bifurcation analysis of the onset of necking in an elastic/plastic cylinder under uniaxial tension, *J. Mech. Phys. Solids*, Vol. 22, pp. 61-71, 1974.
15) Khojastehpour, M., Hashiguchi, K., Plane strain bifurcation analysis of soils by the tangential-subloading surface model, *Int. J. Solids and Struct.* Vol. 41, pp. 5541–5563, 2004.
16) Khojastehpour, M., Hashiguchi, K., Murakami, Y., Axisymmetric bifurcations of metals with tangential-subloading surface model, *J. Appl. Mech. (JSCE)* Vol. 7, pp. 527-534, 2004.
17) Miles, J.P., Bifurcation in plastic flow under uniaxial tension, *J. Mech. Phys. Solids*, Vol. 19, pp. 89-102. 1971.
18) Miles, J.P. and Nuwayhid, U.A., Bifurcation in compressible elastic/plastic cylinders under uniaxial tension, *Appl. Sci. Res.*, Vol. 42, pp. 33-54, 1985.
19) Needleman, A., Non-normality and bifurcation in plane strain tension and compression, *J. Mech. Phys. Solids*, Vol. 27, pp. 231-254, 1979.
20) Rudnicki, J.W. and Rice, J.R., Conditions for localization of deformation in pressure-sensitive dilatant materials, *J. Mech. Phys. Solids*, Vol. 23, pp. 371-394, 1975.
21) Pan, Y.-C, Chou, T.-W., Point force solution for an infinite transversely isotropic solid, *J. Appl. Mech. (ASME)* Vol. 43, pp. 608-612, 1976.
22) Spiegel, M.R. and Liu, J., *Mathematical handbook of formulas and tables*, Schaum's outline series, McGraw-Hill, USA, 1999.
23) Timoshenko, S.P., Gere, J.M., *Theory of elastic stability*, 2nd ed., McGraw-Hill, USA. 1961.
24) Vardoulakis, I., Bifurcation analysis of the plane rectilinear deformation on dry sand samples, *Int. J. Solids Struct.*, Vol. 17, pp. 1085-1101, 1981.
25) Vardoulakis, I., Rigid granular plasticity model and bifurcation in triaxial test, *Acta Mechanica*, Vol. 49, pp. 57-79, 1983.
26) Yatomi, C., Shibi, T., Antisymmetric bifurcation analysis in a cylinder of a non-coaxial Cam-clay model, *In: Proceeding of the International Symposium on Deformation and Progressive Failure in Geomechanics, Nagoya*, pp. 9-14, 1997.
27) Young, N. J. B., Bifurcation phenomena in plane compression test, *J. Mech. Phys. Solids*, Vol. 24, pp. 77-91, 1976.

(Received: April 15, 2005)